How accurate are neural approximations of complex network dynamics?

Vaiva Vasiliauskaite Computational Social Science, ETH Zürich, 8092 Zürich, Switzerland

Nino Antulov-Fantulin*

Computational Social Science, ETH Zürich & Aisot Technologies AG, Zürich, Switzerland

(Dated: October 18, 2023)

Data-driven approximations of ordinary differential equations offer a promising alternative to classical methods of discovering a dynamical system model, particularly in complex systems lacking explicit first principles. This paper focuses on a complex system whose dynamics is described with a system of such equations, coupled through a complex network. Numerous real-world systems, including financial, social, and neural systems, belong to this class of dynamical models. We propose essential elements for approximating these dynamical systems using neural networks, including necessary biases and an appropriate neural architecture. Emphasizing the differences from static supervised learning, we advocate for evaluating generalization beyond classical assumptions of statistical learning theory. To estimate confidence in prediction during inference time, we introduce a dedicated null model. By studying various complex network dynamics, we demonstrate that the neural approximations of dynamics generalize across complex network structures, sizes, and statistical properties of inputs. Our comprehensive framework enables accurate and reliable deep learning approximations of high-dimensional, nonlinear dynamical systems.

Coupled differential equations serve as a fundamental modeling tool for dynamical systems, enabling classical analyses such as stability and control. In its simplest form, a dynamical system is defined as a set of coupled ordinary differential equations $\dot{\mathbf{x}}(t) = \mathcal{F}(\mathbf{x}(t))$ that describe the rate of change of a dependent variable \mathbf{x} . Discovering a dynamical model entails the task of finding a suitable vector field \mathcal{F} , and requires a deep understanding of first principles from disciplines like physics, as well as insights derived from experiments and, above all, creativity.

In today's data-rich world, there is an allure to leverage this abundant resource for synthesizing \mathcal{F} . One popular approach involves utilizing symbolic regression analysis to determine the elementary functions that constitute \mathcal{F} [1–4]. However, these models assume that parsimonious enumeration of the dynamics in terms of known basis functions exists and is possible to determine, which may not always be the case [5], especially if no prior knowledge about a system is available [6]. Furthermore, the system identification task solved by symbolic regression using experimental data is NP-hard for both classical and quantum systems [7, 8].

Instead of identifying the elementary functions that constitute \mathcal{F} , an alternative and appealing method approximates \mathcal{F} using a neural network, denoted as Ψ [9, 10]. Neural networks have been proven useful for various tasks related to dynamical systems, such as control [11–13] and forecasting [14, 15]. However, for the task of approximating the vector field \mathcal{F} , it may be insufficient to only have an expressive neural network. An architecture that disrespects the physical realism of the true dynamical model may lead to an abrupt cut-off

for the domain within which the model performs well. While within the predefined domain, the model's performance is guaranteed by the Universal Approximation Theorems (UAT) [16, 17] and Statistical Learning Theory (SLT) [18, 19], the conditions upon which these theorems are established are violated more often than not when we study dynamical systems in practice. Consequently, dynamical systems lie at the boundary of our current understanding of the power of deep learning.

In this paper, we propose expanding the framework for evaluating the quality of a neural network's generalization beyond the classical boundaries of UAT and SLT. We also define a statistical significance test that is driven by the allowed fluctuations of the model variance, aimed at identifying limitations of neural network generalization capacity.

We concentrate on a sub-domain of dynamical systems known as complex systems. Complex systems are often modelled as networks (graphs) composed of interdependent, internally equivalent elements called agents [20, 21]. The emergent behavior and properties of these systems arise from the local interactions among these agents. Examples of complex systems include ecosystems, economies, the brain, as well as social networks. The change in the state of each agent i, denoted as $\dot{\mathbf{x}}_i(t) \in \mathbb{R}^k$, depends not only on its own state $\mathbf{x}_i(t)$ but also on the sum of the states of its neighbors:

$$\dot{\mathbf{x}}_{i}(t) = L(\mathbf{x}_{i}(t), t) + \bigoplus_{j} A_{ij}(t)Q(\mathbf{x}_{i}(t), \mathbf{x}_{j}(t), t)$$
(1)
$$= \mathcal{F}(\mathbf{x}_{i}(t), \mathbf{x}(t), \mathbf{A}(t), t),$$

where $\mathbf{x}(t) \in \mathbb{R}^{n \times k}$ is a tensor that collects states of all n nodes at time t. This system can be described by n (coupled) ordinary differential equations (ODEs), where $\mathbf{A}(t) \in \mathbb{R}^{n \times n}$ represents a potentially time-varying network adjacency matrix, L is a function that describes

^{*} anino@ethz.ch

self-interactions, Q is a function that models pairwise interactions between neighbors, and \bigoplus denotes an aggregation function. Dynamical systems of arbitrary size and connectivity structure can be described using the same functions L,Q,\bigoplus thereby entailing the same type of dynamics, only on a different network. In this work, we concentrate on a simple case of autonomous dynamics on undirected, unweighted static graphs, but our results could be easily extended to more general cases.

By making appropriate choices for the functions L, Q, and \bigoplus , Eq. 1 can represent a wide variety of models for complex network dynamics [22, 23], including biochemical dynamics, birth-death processes, spreading processes, gene regulatory dynamics [23], as well as chaotic [24], diffusive [25], oscillatory [26], neuronal [27] dynamics. However, it is worth noting that for many complex systems, the dynamical model, i.e., the functional forms of L, Q, and \bigoplus remains unknown, as there are no first principles[28] from which such models can be derived ab initio, making data-driven approaches a particularly alluring option.

The paper is organized as follows. In Sec. I, we introduce a prototype neural network model, denoted as Ψ , designed to approximate the dynamical system \mathcal{F} described by Eq. 1, as well as a general learning setting for the task of approximating \mathcal{F} . In Sec. II, we define a hierarchy of conditions to be met by the model that defines its generalization capacity beyond the limits of SLT. In Sec. III, we outline the statistical significance test that could identify the limit of a neural network's generalization capacity. Using the generalization hierarchy as well as the statistical significance test, in Sec. IV we assess the generalization capacity of the proposed model as well as our ability to mark the boundary beyond which the model is not anymore reliable. Lastly, in Sec. V, we discuss implications of noisy and irregularly sampled real data.

I. A NEURAL NETWORK MODEL

To approximate a dynamical system with a neural network, we need to learn the vector field \mathcal{F} which describes the change in the state of system's variables $\mathbf{x}(t)$. In the case that state of each node is a scalar value e.g. all dynamics in Tab. I, vector field is simply a function $\mathcal{F}: \mathbb{R}^n \to \mathbb{R}^n$. We proceed with the assumption that to approximate dynamics in a complex system, the neural network model which mimics the structure of the right-hand side of Eq. 1 is the most appropriate candidate for the task and propose a novel spatio-temporal constrained version of a graph neural network [29, 30], defined as:

$$\boldsymbol{\Psi}(\mathbf{x}) \ = \ \boldsymbol{\psi}^{\ell}(\mathbf{x}) + \boldsymbol{\psi}^{\bigoplus} \left[\mathbf{A} \odot \left(\boldsymbol{\psi}^{q_1}(\mathbf{x})^{\top_1} \times_b \boldsymbol{\psi}^{q_2}(\mathbf{x})^{\top_2} \right) \right] (2)$$

Here $\psi(\cdot)$ is a feed forward neural network with one or more hidden layers $\{\mathbf{h}^1, \mathbf{h}^2, ..., \mathbf{h}^N\}$ of the form $\psi(\mathbf{h}^{i+1}) = \sigma(\mathbf{h}^i \mathbf{W} + \mathbf{b}), \mathbf{h}^1 = \mathbf{x}$; an operator \odot denotes a standard "broadcasted" element-wise multiplication,

while \times_b indicates a "batched" matrix-matrix product, and \top_1, \top_2 specific transpose operations. Sec. I of the Supporting Information (SI) includes a detailed description of the architecture.

Let us review the set of inductive biases, tailored specifically for complex network dynamics, that we considered in designing the architecture of Ψ . First, we assumed that dynamics on a complex network is size**invariant**, i.e. networks of various size and topology can, in principle, sustain the same type of dynamics. To achieve the size-invariance, we require Ψ to be composed of element-wise functions ψ^{ℓ} , ψ^{q_1} , and ψ^{q_2} . Additionally, we assumed that \mathcal{F} is expressed as a sum of two types of independent interactions: neighbor interactions and self-interactions (corresponding respectively to Q and L in Eq. 1). Moreover, we incorporate an invariant pooling layer within the ψ^{\oplus} operation to maintain the invariance with respect to the order of inputs [31–33] when summing over the neighbor interaction terms. Lastly, we note that Eq. 1 assumes only local (neighbor interactions), that is, per infinitesimal amount of time, a signal may only propagate from one neighbor to another. Interactions between $\kappa^{\rm th}$ neighbors would be encoded with terms coupled through \mathbf{A}^{κ} , $(\kappa > 1)$. To ensure spatio-temporal locality, we opted to forego multiple graph convolution layers [29, 30] and use the adjacency matrix A solely as an input.

Learning setting The training and test data are defined as $\mathcal{D} = \{(\mathbf{x}, \mathbf{y})\}$, s.t. $\mathbf{x} \in \mathbb{R}^{n \times k}, \mathbf{y} \in \mathbb{R}^{n \times k}$. The best neural approximation $\mathbf{\Psi}^*$ is obtained by minimizing the loss \mathcal{L} between the true labels \mathbf{y} and the predicted labels $\hat{\mathbf{y}}$ in the training data:

$$\begin{split} \boldsymbol{\Psi}^* &= \arg \min_{\boldsymbol{\Psi}: \mathbb{R}^{n \times k} \to \mathbb{R}^{n \times k}} \underset{\mathcal{P}(\mathbf{x}, \mathbf{y})}{\mathbb{E}} \mathcal{L}(\hat{\mathbf{y}}, \mathbf{y}), \\ &\text{where } \hat{\mathbf{y}} = f(\boldsymbol{\Psi}, \mathbf{x}, \boldsymbol{\theta}), \end{split}$$

and $\boldsymbol{\theta}$ are non-trainable parameters necessary to estimate $\hat{\mathbf{y}}$, e.g. adjacency matrix \mathbf{A} . In the subsequent sections, we will omit the superscript "*" and refer to the best model obtained after training as $\boldsymbol{\Psi}$. The results presented in the subsequent sections were obtained using the normalized ℓ^1 norm:

$$\mathcal{L} = \frac{1}{Z} \Big[\mathbf{E}_{(\mathbf{x}, \mathbf{y}) \in \mathcal{D}} \Big[\| \mathbf{y} - f(\mathbf{\Psi}, \mathbf{x}, \boldsymbol{\theta}) \|_{1} + \lambda \mathbf{Var}_{i} \| \mathbf{y}_{i} - f_{i}(\mathbf{\Psi}, \mathbf{x}, \boldsymbol{\theta}) \|_{1} \Big] \Big],$$
(3)

where $\|\cdot\|_1$ denotes the ℓ^1 norm and the normalization Z=nk. The loss per each sample, or node, can be further weighed to reduce bias towards optimizing for common nodes at a cost of poor predictions at rare nodes [10]. Instead of such weighting, we adopt a regularizer that penalizes solutions with high variance in the loss across nodes, without a priori defining which nodes are important.

In Sec. IV, we will consider a case where labels originate from a vector field $\mathbf{y} = \mathcal{F}(\mathbf{x})$ and $\hat{\mathbf{y}} = \mathbf{\Psi}(\mathbf{x})$, whereas in Sec. V, we will discuss training with labels derived from

noisy trajectories: $\mathbf{y} = I[\mathbf{\mathcal{F}}, \mathbf{x}, \mathbf{A}, t_1, t_2] + \boldsymbol{\varepsilon}$ and predicted labels defined as $\hat{\mathbf{y}} = I[\mathbf{\Psi}, \mathbf{x}, \mathbf{A}, t_1, t_2]$. Here $\boldsymbol{\varepsilon}$ denotes observational noise, and numerical integration is denoted as

$$I[g, \mathbf{x}, t_1, t_2] = \mathbf{x} + \int_{t_1}^{t_2} g(\mathbf{x}', \mathbf{A}) d\tau.$$

Note that the time step $d\tau$ in the numerical integration may be different for the true and the predicted labels.

Let us further denote probability density functions associated with a training setting by ϕ , and with a test setting by ω . For training, we consider two types of datasets: $\mathbf{x} \sim \phi_x(\mathbf{x})$ are i.i.d. samples from a pre-defined distribution, or non-i.i.d. samples $\{\mathbf{x}(t)\}$ obtained by numerical integration $\mathbf{x}(t) = I[\mathbf{F}, \mathbf{x}_0, t_0, t]$ with a random initial condition $\mathbf{x}_0 \sim \phi_{x_0}(\mathbf{x})$. Replacing ϕ by ω , defines test datasets.

II. GENERALIZATION HIERARCHY

The attractiveness of the deep learning approach lies in the fact that multilayer feed-forward neural networks with arbitrary width are universal function approximators [16, 17] according to the universal approximation theorem (UAT). It holds for various deep neural networks including those with arbitrary depth [34, 35], bounded depth and width [36], and permutation invariant neural networks operating on sets or graphs [31–33].

While UAT guarantees that a function can be approximated, it does not provide insights into the generalization capacity of trained models with respect to the new data. The generalization in machine learning is typically studied through the lens of statistical learning theory (SLT) [18, 19]. In SLT, the training and test data consist of input-label pairs, drawn from unknown probability distributions. For not over-parameterized models, SLT states that if the training and test data are independently and identically distributed (i.i.d.) samples, the training loss serves as a reasonable proxy for the test loss, guaranteeing that the model generalizes well to unseen test data. The uniform convergence theorems [37] offer various bounds on the difference between training error and test error.

Generalization of neural networks, particularly when used to approximate dynamical systems, deserves a closer look. Firstly, neural networks belong to the class of overparameterized models, which are currently not fully understood within classical SLT [38–40][41]. SLT also offers no performance guarantees when the statistical properties of the test data deviate from those of the training data. Since for the task of approximation of dynamics, real training data would be in the form of non-i.i.d. time series trajectories that likely do not comprehensively cover the state space, it remains unclear whether such data is adequate to reconstruct \mathcal{F} . Lastly, when the support of the test data is not equivalent to the support of the training data, UAT is no longer valid, since it is built

upon an assumption that a function being approximated has a compact support [42].

A neural network model should arguably explain dynamics not only within its training setting, but also extrapolate to a different dynamical system, where interaction rules are preserved, yet it is different in terms of who interacts with whom, or the number of interacting units. With this in mind, we propose to evaluate the trained models at several distinct levels of generality in terms of the model's inputs, extending the limits of UAT and SLT. Particularly for models of complex network dynamics, the change in state is governed by the state itself, as well as the connectivity between nodes. Therefore, we propose to consider generality in two directions: in terms of statistical properties of the dataset \mathcal{D} , or of the graph, mathematically represented as an adjacency matrix A. In both cases, the accuracy of a model, e.g. loss, is contrasted to increasing differences in these inputs during training and testing.

Input data A model should be able to extrapolate to unseen input datapoints which are sampled from the same probability distribution function as training data: $\phi(\mathbf{x}) \equiv \omega(\mathbf{x})$. This is the basic level of generalization that is also covered by SLT. At a higher level of generality, we relax the equivalence $\phi(\mathbf{x}) \not\equiv \omega(\mathbf{x})$, however $\operatorname{supp} \left[\phi(\mathbf{x}) \right] = \operatorname{supp} \left[\omega(\mathbf{x}) \right]$, injecting some amount of statistical dissimilarity between the training and test data, but keeping the support of corresponding random variables equal. Lastly, one can relax all constraints on the statistical properties of inputs, defining the topmost level of generality. It is worth noting that the last condition is typically absent in traditional machine learning approaches, as an input standardization step ensures that the model never receives inputs outside the range of values it was trained on [43]. However, in the context of dynamical systems, standardization would modify the dynamics' outcomes and break connections to physical reality, as distinct inputs would be non-injectively mapped to the same standardized values.

Graph structure At the most fundamental level, the model's generalization encompasses its ability to approximate dynamics on a different graph that bears high resemblance to the original graph. Here we consider another graph from the canonical ensemble [44] of the original graph: $\phi(\mathbf{A}) \equiv \omega(\mathbf{A})[45]$. By further relaxing constraints and allowing for the probability distributions to differ, and for size of the training and the test graph to vary, we study the extent to which the model generalizes to a grand-canonical ensemble. We propose that the former constraint corresponds to a mid-level of generalization, while the latter represents the highest level. These tests not only prove valuable in assessing the model's accuracy but also indicate how useful neural approximations are for modeling dynamics on systems of varied size and connectivity.

III. STATISTICAL SIGNIFICANCE

When a neural network model is used for forecasting and extrapolating to unseen inputs or unseen topologies, there is no ground truth to contrast the prediction against. As a means to gauge the representativeness of the prediction, we suggest using a statistical hypothesis test, based on a dedicated null model.

Null model Let us consider an ensemble $\{\Psi_m\}$ of overparameterized neural networks that are trained on bootstrapped versions of training data \mathcal{D} . Each Ψ_m is a realization of a random variable, where the sources of randomness are the stochastic nature of the optimization algorithm and the initialization of weights. Our ansatz is that an ensemble of neural networks disagrees more on the estimate of the vector field \mathcal{F} as the test samples diverge from the training samples. Fig. 1 shows an example of such behaviour, where the variance of overparameterized neural networks $\{\Psi_m\}$ indeed increased once we departed from the training range.

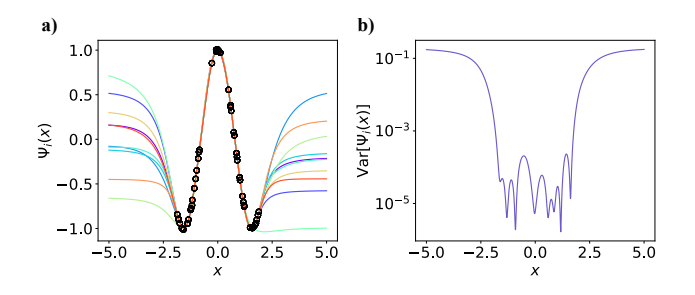


FIG. 1. An ensemble of 10 overparameterized feed forward neural networks $\{\Psi_m(x)\}$ trained independently to approximate $\mathcal{F}(x) = \cos 2x$ within the range [-2,2] (50 training samples are indicated with black circles). a) Predictions of the models outside the training range, $x \in [-5,5]$. b) Sample variance across ensemble of neural networks $\{\Psi_m(x)\}$.

d-statistic One possible statistic to quantify acceptable amount of model variance is the variance across neural networks in the prediction of ith node's derivative i.e. $d(\mathbf{x}_i) = \mathrm{Var}(\mathbf{\Psi}_m(\mathbf{x}_i))$ — the variance term in the biasvariance decomposition [46]. In the case that the node state variable \mathbf{x}_i is multi-dimensional (k > 1, but not too large), one can generate the null distribution $f_d(\xi)$ and perform a statistical test for each dimension separately.

To estimate the d-statistic, we first train a total of M neural networks using, for each, a different bootstrapped sample of the same dataset \mathcal{D} . The distribution of d-statistic, $f_d(\xi)$ is then obtained by repeatedly taking a size m sub-sample of neural networks and computing a d-statistic of some input \mathbf{x}_i . By analyzing variance in such a bootstrapped dataset, we estimate the effect of changes in the training data on the estimated models, thereby performing a form of stability analysis.

Significance test Since we expect the variance across models to increase, i.e. to fall to the right of the null distribution $f_d(\xi)$, an appropriate significance test is

right-tailed. A null hypothesis H_0 tests whether, for a given test data point \mathbf{x}_i^* , a corresponding value of the d-statistic, d^* comes from a null distribution $f_d(\xi)$ that is generated by the null model. We reject this hypothesis if the p-value, defined as

$$p := 1 - \int_0^{d^*} f_d(\xi) d\xi \equiv \int_{d^*}^{\infty} f_d(\xi) d\xi \le \alpha, \qquad (4)$$

where we set $\alpha = 0.05$ in the discussed analysis.

The significance test cannot tell whether the estimated derivative is close to the ground truth derivative, as the test does not estimate the bias term in bias-variance decomposition. Nevertheless, as is evident in Fig. 1 and Fig. 2 discussed in the next section, the d-statistic is correlated with the average loss on the test dataset. As the total error can be decomposed into the variance and bias terms, high variance necessarily indicates high error. The opposite, however, is not necessarily true, since an ensemble of models could be very certain about a very wrong prediction.

IV. APPROXIMATIONS OF MODELS FOR COMPLEX NETWORK DYNAMICS

To study the generalization capacity of the neural network model presented in Sec. I, we consider a graph sampled from an Erdös-Rényi (ER) network ensemble with n=100 nodes and a probability of an edge of p=0.1 [47]. We simulate five different types of dynamics: mass-action kinetics (MAK), population dynamics (PD), Michaelis-Menten (MM) equation, susceptible-infected-susceptible (SIS) model discussed in [23], as well as heat diffusion (Heat) [48]. The true functional forms and parameters of the dynamics are listed in Tab. I. SI includes a detailed description of the parameters used in the training procedure.

Tab. I compares the loss, Eq. 3 in the training data to the loss in the test data. From the left, the first two columns present a model's capacity to generalize when the test input has the same statistical properties as the training data ($\mathbf{x} \sim \mathcal{U}(0,1)$) and when it is sampled from a different distribution ($\mathbf{x} \sim \mathcal{B}(5,2)$). The last two columns present the generalization capacity in the graph dimension. First, we sample a network \mathcal{H} from the ensemble of the training graph $\mathcal{G}(\mathcal{H} \sim \mathcal{P}(\mathfrak{G}))$. In the final column, we alter the network ensemble by adjusting the edge probability to p = 0.6. $(\mathcal{H} \sim \mathcal{P}(\mathfrak{H}))$. The results in the table confirm that a neural network can approximate \mathcal{F} and generalize to inputs sampled from an unseen distribution. Further results presented in Fig. S3 of SI confirm that this result is stable for a variety of input's distributions with a support equivalent to that of the training data.

The trained models can also make accurate predictions on graphs that are from the same canonical ensemble. The loss observed for a graph from a different network

Dynamics	L	Q	$\mathbf{x} \sim \mathcal{U}(0,1)$	Test data $\mathbf{x} \sim \mathcal{U}(0,1)$ $\mathcal{G} \equiv \mathcal{H}$	$\mathbf{x} \sim \mathcal{B}(5,2)$	$\mathbf{x} \sim \mathcal{U}(0,1)$	$\mathbf{x} \sim \mathcal{U}(0, 1)$
Heat	-	$B(x_j - x_i)$	0.95 ± 0.88	0.95 ± 0.88	0.63 ± 0.51	0.98 ± 0.04	5.19 ± 0.06
MAK	$F - Bx_i^b$	ï	1.14 ± 1.34				
MM	$-Bx_i$	$R\frac{x_j^n}{1+x_j^h}$	2.54 ± 1.95	2.55 ± 1.96	2.02 ± 1.56	2.61 ± 0.06	6.7 ± 0.1
PD SIS	$ \begin{array}{l} -Bx_i^b \\ -Bx_i \end{array} $	$Rx_j^{a^j}$ $R(1-x_i)x_j$	2.62 ± 1.87	2.61 ± 1.86	3.16 ± 2.0	2.68 ± 0.05	10.87 ± 0.15

TABLE I. Generalization of a neural network model with respect to input data or a graph. The models were trained to approximate dynamics of the form Eq. 1. The loss, defined in Eq. 3, is multiplied by 10^2 . In all cases, $|\mathcal{H}| = |\mathcal{G}|$, where \mathcal{G} is the graph used in training, and \mathcal{H} is the test graph. The first results column from the left reports training loss, which, contrasted to test losses indicates that the neural network models generalize well under the constraint that the test data has equivalent support to the training data, and the training and test graphs are of the same size.

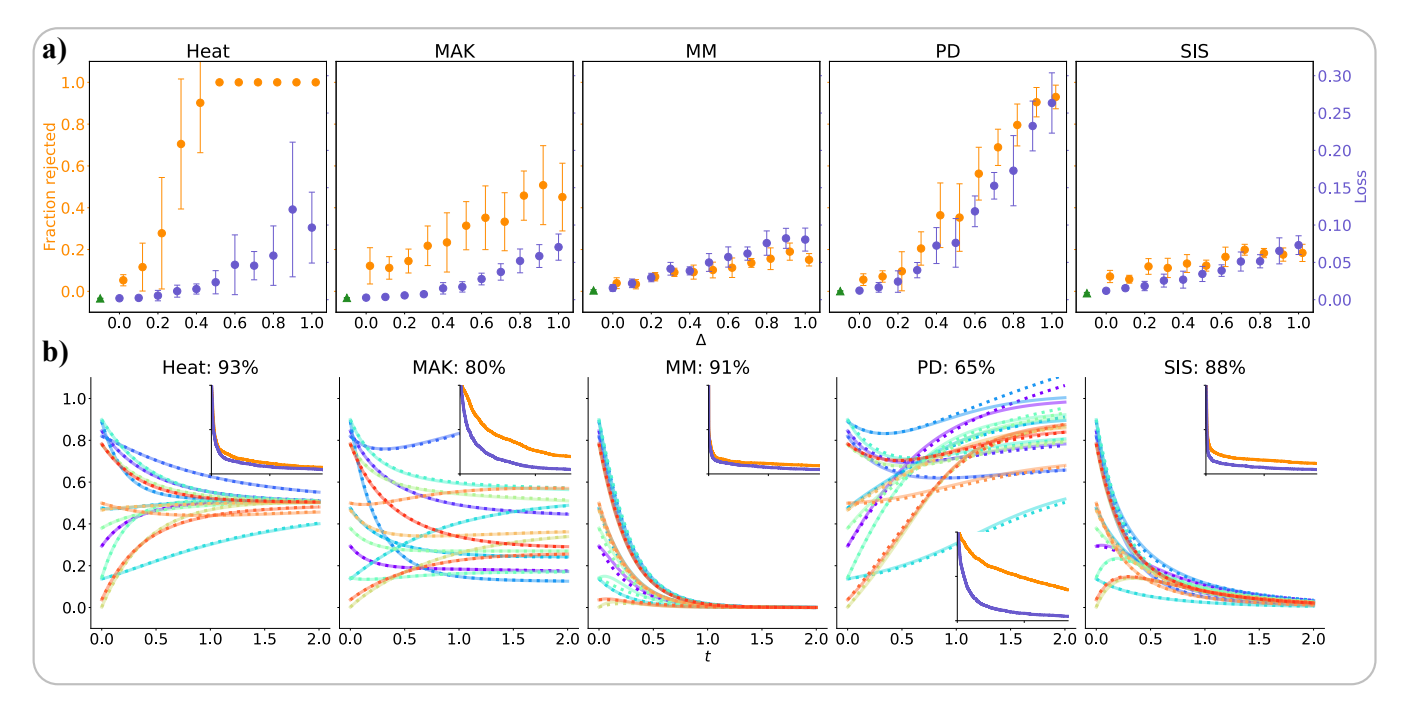


FIG. 2. Significance test applied to the five complex network dynamics. In both **a)** and **b)** a set of 50 neural networks were trained on data from one time series trajectory set, where dynamics evolved on a random graph with p=0.5 and initial conditions were sampled from $\mathcal{U}(0,1)$. The training graph has n=10 nodes. **a)** compares the training loss (green triangle) with the test loss (purple circles), as a function of Δ , where the initial value $\mathbf{x}(t_0) \sim \mathcal{U}(0,1) + \Delta$. The orange circles indicate the fraction of rejected data points based on the d-statistic for a given Δ . Here the test graph is isomorphic to the training graph. In **b)**, we changed the test graph to a larger one, n=15, p=0.3 and contrast the true dynamics (solid lines) and the neural network predictions (dotted lines) for a new set of initial values that are sampled from the training distribution. The insets contrast the cumulative distribution of the d-statistic in training data (purple) and in test data (orange) and show the distributions in the range up to a critical value for the significance level of 5%. The title reports the percentage of accepted data points, i.e. the percentage of datapoints for which the corresponding d-statistic fell within the 95% of the null (purple) distribution.

ensemble is, however, significantly larger than the training loss, suggesting the limit of the trained model's applicability. However, the magnitude of the loss for a node correlates with the node's degree due to the summation of neighbor interaction terms, possibly causing increase in the loss observed when the model was applied to make predictions in a denser graph. Fig. S4a) of SI indicates that this dependence is monotonically increasing with the

density of a graph, confirming this intuition. Tab. S1 in SI reports the error in approximating the self-interaction term and the aggregate of the neighbor-interaction terms separately, and shows that indeed, the increase in loss is due to accumulation of errors in the neighbor interaction term. In future, it will be important to develop a framework which allows to remove this neighborhood-size dependence.

When the support of the test input data departs from the support of training data, the loss increases monotonically, as is shown in Fig. 2a). Importantly, the d-statistic is an informative proxy of this trend. The exact reasons of this correlation fall outside the scope of the paper, however we conjecture that it may be explained by special regularities present in the class of functions used in dynamical systems, namely Lipschitz continuous. As neural networks have a spectral learning bias towards low frequencies [49–51], some part of the generalization out-of-range may be due to the dominance of low frequencies in the decomposition of functions $\mathcal F$ we considered.

Furthermore, Fig. 2b) shows that neural network models trained using a graph of size n may also be repurposed to describe dynamics on a larger graph. The accuracy varies across different models of dynamics, and the d-statistic reflects these differences. Fig. S4 b) and c) of SI show more granular results in terms of the size of the test graph and shift Δ in values of test inputs with respect to the support of training data.

Overall, the neural networks can approximate various dynamical models well, and extrapolate predictions even when statistical properties of the input data, or the graph structure change, transcending the formal boundaries of SLT and UAT. As expected, there is indeed a limit for how much generalization can be achieved, however, we note the presence of regularity that is observed in the increase in test loss, as mentioned in Sec. III. Using the proposed d-statistic we can therefore evaluate the confidence in the inferred prediction, even in cases when we depart from standard SLT, UAT assumptions of i.i.d. sampling and a compact support.

V. USE OF REAL DATA

So far, we have operated with an assumption that the training data is not noisy and \mathcal{F} is available. In real-world, the training data will likely come in the form of time series $\{\mathbf{x}(t)\}$ sampled at potentially irregular intervals. Here $\mathbf{x}(t)$ is an observable, but $\dot{\mathbf{x}} = \mathcal{F}(\mathbf{x})$ is not. The dataset derived from time series would consist of non-i.i.d. samples and would exhibit heterogeneous coverage of the state space. Real systems are also subject to observational noise: assuming additive noise, the observed signal is $\mathbf{z}[\mathbf{x}(t)] = \mathbf{x}(t) + \boldsymbol{\varepsilon}(t)$.

If the exact sampling times are known, e.g. we collect R signal samples $\mathbf{x}(t_r)$, $t_r \in \{t_0, t_1, ..., t_R\}$, then it is sufficient to construct the labels in the training data as $\mathbf{y} = \dot{\mathbf{x}}_r \approx \frac{\mathbf{x}(t_{r+1}) - \mathbf{x}(t_r)}{\delta_r}$, where $\delta_r = t_{r+1} - t_r$. If $\delta_r = \delta$ $\forall r$, we can continue with training as before. The neural model Ψ_{δ} is then valid at this δ and would potentially diverge for smaller values of δ .

If δ_r is time-varying, one should learn Ψ at a much higher frequency Δt to allow estimates $\mathbf{x}(t_r)$, i.e. $\hat{\mathbf{x}}(t_r)$ from $\mathbf{x}(t_{r-1})$ using numerical integration. We set $\delta_r \gg \Delta t$ so that $\frac{\delta_r}{\Delta t} \approx 0 \ \forall r$. All in all, the procedure is illus-

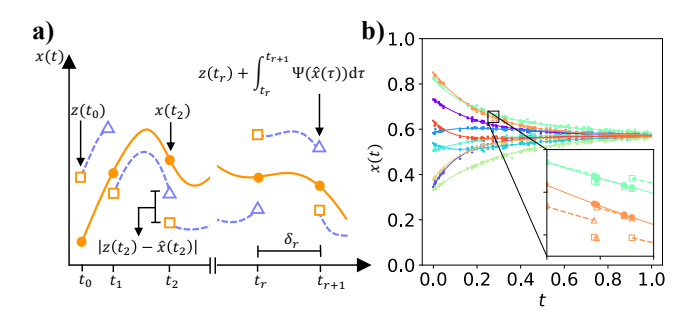


FIG. 3. a) Illustration of training a neural network from irregularly sampled one dimensional signal $x(t_r),\ t_r\in[0,R]$ (orange solid line). True labels are the observed signal $z(t_r)$, compared during training to predicted labels $\hat{x}(t_r)=z(t_{r-1})+\int_{t_{r-1}}^{t_r}\Psi(\hat{x}(\tau))\mathrm{d}\tau.$ Here the integral is evaluated numerically using infinitesimal time Δt . b) shows neural network approximations of heat diffusion dynamics when a noisy, irregularly sampled signal used in training. In the inset, the square scatter points indicate the temporary initial values which are inputs to the neural network, whereas the triangles represent the predicted labels.

trated in Fig. 3a) and uses the following loss function:

$$\mathcal{L} = \sum_{r=0}^{R} \left\| \mathbf{z}[\mathbf{x}(t_r)] - \mathbf{z}[\mathbf{x}(t_{r-1})] - \int_{t_{r-1}}^{t_r} \mathbf{\Psi}(\hat{\mathbf{x}}(\tau)) d\tau \right\|_{1}.$$

Here the gradient descent is computed through a forward computational graph, employing an ODE solver. For efficiency, an adjoint sensitivity method could also be used [52, 53]. We review the computational graph and the gradient update rule in Sec. VII of SI.

Fig. 3b) shows an example of training the neural network to approximate heat diffusion from irregularly sampled, noisy time series data. Approximating the rate of change in the system state is possible even in a realistic setting where the state variables are observed with noise and at irregular sampling intervals. To test the effect of noise, we trained another neural network using the same data without observational noise. We then considered a test loss $\mathbf{E}_{\mathcal{D}:\mathbf{x}\sim\phi_{x_0}(\mathbf{x})}[\|\hat{\mathbf{x}}(\delta)-\mathbf{x}(\delta)\|_1]$, where $\hat{\mathbf{x}}(\delta)$ is a prediction, obtained by numerically integrating $\mathbf{\Psi}$ starting with x from t=0 to $t=\delta$, using Δt as an infinitesimal timestep and \mathbf{x} as an initial value, and $\mathbf{x}(\delta)$ is obtained in the same manner using \mathcal{F} . The resulting test loss are not significantly different between the models (respectively, 0.068 ± 0.022 for the model with noise and 0.069 ± 0.02 for the model without the noise). As a contrast, an random untrained neural network yielded a significantly larger loss of 0.141 ± 0.034 . Therefore, learning with time series data is possible, and a neural network trained with noisy data can achieve comparable accuracy to a model trained with noiseless data.

CONCLUSION AND DISCUSSION

We presented a comprehensive framework to approximate a dynamical system of ordinary differential equations coupled via a complex network (graph), a ubiquitous model of dynamics in complex systems. We introduced a toolbox to analyze the quality of neural approximations with the standard ruler of statistical learning theory, as well as in more diverse settings: (i) when statistical properties for train and test data differ, (ii) data samples are non-i.i.d., and (iii) the ground truth functions have a non-compact support. When a model accurately resembles the true functional form of the dynamics, the trained model is not only expressive within the conditions that it was trained on, but also has potential to generalize beyond boundaries set out by UAT and by SLT. To gauge confidence in the inferred predictions within these diverse test settings, we entrained a dedicated null model and a statistical test.

The set of tools we have presented could be extended to understand both the limits and benefits of deep learning models for complex dynamical systems. While we observed some generalization capacity, we note that there is an accumulation of errors in the approximation of neighbour interactions term that is neighbourhood size-dependent. Furthermore, if the functions that constitute \mathcal{F} , namely, L and Q are not learnt accurately, the model's generalization is impeded. More exotic training settings hold potential to help resolve these issues. We also suggest studying neural trainability through the

property of dynamic isometry and the mean-field theory [54, 55], enforcing physical constraints e.g. Lipschitz continuity of dynamics [56], and expanding the range of tools from SLT [38–40]. We also limited our analysis to the simplest case where the dynamics is deterministic and autonomous, and the graphs are static, undirected, connected and fully known. It will be important to study the effects of increased complexity of the structure on the approximations. Lastly, in future it will be important to better understand how the state space coverage impacts the accuracy of model's predictions in-sample as well as out-of-sample.

More broadly, we emphasize that applications of deep learning models of dynamical system go beyond mere predictions within statistical confines of training data. Therefore it is imperative that these models be constructed to maintain accuracy with conditions, that were not encountered during training, e.g. when test data has a different support to training data. Expanding our proposed framework holds a potential of enabling forecasting, modeling and, ultimately, understanding a wide spectrum of complex dynamical systems.

ACKNOWLEDGEMENTS

This work is supported by the European Union – Horizon 2020 Program under the scheme "INFRAIA-01-2018-2019 – Integrating Activities for Advanced Communities", Grant Agreement n.871042, "SoBigData++: European Integrated Infrastructure for Social Mining and Big Data Analytics" (http://www.sobigdata.eu).

- S. L. Brunton, J. L. Proctor, J. N. Kutz, and W. Bialek, Discovering governing equations from data by sparse identification of nonlinear dynamical systems, Proceedings of the National Academy of Sciences of the United States of America 113, 3932 (2016).
- [2] T.-T. Gao and G. Yan, Autonomous inference of complex network dynamics from incomplete and noisy data 10.1038/s43588-022-00217-0.
- [3] S.-M. Udrescu and M. Tegmark, Ai feynman: A physicsinspired method for symbolic regression, Science Advances 6, eaay2631 (2020).
- [4] M. Schmidt and H. Lipson, Distilling free-form natural laws from experimental data, science 324, 81 (2009).
- [5] W. Gilpin, Y. Huang, and D. B. Forger, Learning dynamics from large biological data sets: machine learning meets systems biology, Current Opinion in Systems Biology 22, 1 (2020).
- [6] C. Hillar and F. Sommer, Comment on the article" distilling free-form natural laws from experimental data", arXiv preprint arXiv:1210.7273 (2012).
- [7] T. S. Cubitt, J. Eisert, and M. M. Wolf, Extracting dynamical equations from experimental data is np hard, Phys. Rev. Lett. 108, 120503 (2012).
- [8] M. Virgolin and S. P. Pissis, Symbolic regression is np-

- hard, arXiv preprint arXiv:2207.01018 (2022).
- [9] C. Zang and F. Wang, Neural Dynamics on Complex Networks, in Proceedings of the ACM SIGKDD International Conference on Knowledge Discovery and Data Mining (Association for Computing Machinery, 2020) pp. 892–902.
- [10] C. Murphy, E. Laurence, and A. Allard, Deep learning of contagion dynamics on complex networks, Nature Communications 12, 10.1038/s41467-021-24732-2 (2021).
- [11] L. Böttcher, N. Antulov-Fantulin, and T. Asikis, Ai pontryagin or how artificial neural networks learn to control dynamical systems, Nature communications 13, 1 (2022).
- [12] T. Asikis, L. Böttcher, and N. Antulov-Fantulin, Neural ordinary differential equation control of dynamics on graphs, Physical Review Research 4, 013221 (2022).
- [13] W. Jin, Z. Wang, Z. Yang, and S. Mou, Pontryagin differentiable programming: An end-to-end learning and control framework, Advances in Neural Information Processing Systems 33, 7979 (2020).
- [14] K. Srinivasan, N. Coble, J. Hamlin, T. Antonsen, E. Ott, and M. Girvan, Parallel Machine Learning for Forecasting the Dynamics of Complex Networks, Physical Review Letters 128, 10.1103/PhysRevLett.128.164101 (2022).
- [15] J. Pathak, B. Hunt, M. Girvan, Z. Lu, and E. Ott, Model-

- free prediction of large spatiotemporally chaotic systems from data: A reservoir computing approach, Physical review letters **120**, 024102 (2018).
- [16] K. Hornik, M. Stinchcombe, and H. White, Multilayer feedforward networks are universal approximators, Neural networks 2, 359 (1989).
- [17] G. Cybenko, Approximation by superpositions of a sigmoidal function, Mathematics of Control, Signals and Systems 5, 455 (1992).
- [18] V. Vapnik and A. Chervonenkis, The necessary and sufficient conditions for consistency in the empirical risk minimization method, Pattern Recognition and Image Analysis 1, 283 (1991).
- [19] P. L. Bartlett and S. Mendelson, Rademacher and gaussian complexities: Risk bounds and structural results, Journal of Machine Learning Research 3, 463 (2002).
- [20] S. Boccaletti, V. Latora, Y. Moreno, M. Chavez, and D.-U. Hwang, Complex networks: Structure and dynamics, Physics reports 424, 175 (2006).
- [21] V. Vasiliauskaite and F. E. Rosas, Understanding complexity via network theory: a gentle introduction, arXiv preprint arXiv:2004.14845 (2020).
- [22] J. P. Gleeson, Binary-state dynamics on complex networks: Pair approximation and beyond, Physical Review X 3, 021004 (2013).
- [23] B. Barzel and A. L. Barabási, Universality in network dynamics, Nature Physics 2013 9:10 9, 673 (2013).
- [24] J. C. Sprot, Chaotic dynamics on large networks, Chaos: An Interdisciplinary Journal of Nonlinear Science 18, 023135 (2008).
- [25] J.-C. Delvenne, R. Lambiotte, and L. E. Rocha, Diffusion on networked systems is a question of time or structure, Nature communications 6, 7366 (2015).
- [26] F. A. Rodrigues, T. K. D. Peron, P. Ji, and J. Kurths, The kuramoto model in complex networks, Physics Reports 610, 1 (2016).
- [27] M. I. Rabinovich, P. Varona, A. I. Selverston, and H. D. Abarbanel, Dynamical principles in neuroscience, Reviews of modern physics 78, 1213 (2006).
- [28] Such as the principle of relativity that leads to, e.g. the mass-energy equivalence.
- [29] F. Scarselli, M. Gori, A. C. Tsoi, M. Hagenbuchner, and G. Monfardini, The graph neural network model, IEEE Transactions on Neural Networks 20, 61 (2009).
- [30] K. Xu, S. Jegelka, W. Hu, and J. Leskovec, How Powerful are Graph Neural Networks?, 7th International Conference on Learning Representations, ICLR 2019 10.48550/arxiv.1810.00826 (2018).
- [31] E. Wagstaff, F. B. Fuchs, M. Engelcke, M. A. Osborne, and I. Posner, Universal approximation of functions on sets, The Journal of Machine Learning Research 23, 6762 (2022).
- [32] M. Zaheer, S. Kottur, S. Ravanbakhsh, B. Poczos, R. R. Salakhutdinov, and A. J. Smola, Deep sets, Advances in neural information processing systems 30 (2017).
- [33] K. Xu, W. Hu, J. Leskovec, and S. Jegelka, How powerful are graph neural networks?, arXiv preprint arXiv:1810.00826 (2018).
- [34] D. Yarotsky, Error bounds for approximations with deep relu networks, Neural Networks 94, 103 (2017).
- [35] P. Kidger and T. Lyons, Universal approximation with deep narrow networks, in *Conference on learning theory* (PMLR, 2020) pp. 2306–2327.
- [36] V. Maiorov and A. Pinkus, Lower bounds for approxi-

- mation by mlp neural networks, Neurocomputing **25**, 81 (1999).
- [37] H. G. Tucker, A generalization of the glivenko-cantelli theorem, The Annals of Mathematical Statistics 30, 828 (1959).
- [38] M. Belkin, D. Hsu, S. Ma, and S. Mandal, Reconciling modern machine-learning practice and the classical biasvariance trade-off, Proceedings of the National Academy of Sciences 116, 15849 (2019).
- [39] C. Zhang, S. Bengio, M. Hardt, B. Recht, and O. Vinyals, Understanding deep learning (still) requires rethinking generalization, Communications of the ACM 64, 107 (2021).
- [40] D. Jakubovitz, R. Giryes, and M. R. Rodrigues, Generalization error in deep learning, in Compressed Sensing and Its Applications: Third International MATHEON Conference 2017 (Springer, 2019) pp. 153–193.
- [41] Novel SLT frameworks, including algorithm stability [57, 58], algorithm robustness [59], PAC-Bayes theory [60, 61], compression and sampling [62, 63] are active fields of research and could possibly shed light on generalization in this class of models.
- [42] Some UAT results cover density in non-compact domains, e.g. [35]. Nonetheless, the authors proceeded with the assumption that a target function maps to zero outside of a given support.
- [43] H. Anysz, A. Zbiciak, and N. Ibadov, The influence of input data standardization method on prediction accuracy of artificial neural networks, Procedia Engineering 153, 66 (2016).
- [44] G. Bianconi, Entropy of network ensembles, Physical Review E 79, 036114 (2009).
- [45] Alternatively, one may consider a micro-canonical ensemble by employing, e.g. a configuration model [64], thereby imposing harder constraints of fixed number of edges.
- [46] T. Hastie, R. Tibshirani, J. H. Friedman, and J. H. Friedman, The elements of statistical learning: data mining, inference, and prediction, Vol. 2 (Springer, 2009).
- [47] P. Erdős, A. Rényi, et al., On the evolution of random graphs, Publ. math. inst. hung. acad. sci 5, 17 (1960).
- [48] M. Newman, *Networks* (Oxford university press, 2018).
- [49] N. Rahaman, A. Baratin, D. Arpit, F. Draxler, M. Lin, F. Hamprecht, Y. Bengio, and A. Courville, On the spectral bias of neural networks, in *International Conference* on Machine Learning (PMLR, 2019) pp. 5301–5310.
- [50] B. Ronen, D. Jacobs, Y. Kasten, and S. Kritchman, The convergence rate of neural networks for learned functions of different frequencies, Advances in Neural Information Processing Systems 32 (2019).
- [51] Z.-Q. J. Xu, Y. Zhang, and Y. Xiao, Training behavior of deep neural network in frequency domain, in Neural Information Processing: 26th International Conference, ICONIP 2019, Sydney, NSW, Australia, December 12– 15, 2019, Proceedings, Part I 26 (Springer, 2019) pp. 264–274.
- [52] L. S. Pontryagin, Mathematical theory of optimal processes (CRC press, 1987).
- [53] R. T. Chen, Y. Rubanova, J. Bettencourt, and D. K. Duvenaud, Neural ordinary differential equations, Advances in neural information processing systems 31 (2018).
- [54] M. Chen, J. Pennington, and S. Schoenholz, Dynamical isometry and a mean field theory of rnns: Gating enables signal propagation in recurrent neural networks, in *International Conference on Machine Learning* (PMLR,

- 2018) pp. 873-882.
- [55] J. Pennington, S. Schoenholz, and S. Ganguli, Resurrecting the sigmoid in deep learning through dynamical isometry: theory and practice, Advances in neural information processing systems 30 (2017).
- [56] H. Gouk, E. Frank, B. Pfahringer, and M. J. Cree, Regularisation of neural networks by enforcing Lipschitz continuity, Machine Learning 110, 393 (2021).
- [57] M. Hardt, B. Recht, and Y. Singer, Train faster, generalize better: Stability of stochastic gradient descent, in International conference on machine learning (PMLR, 2016) pp. 1225–1234.
- [58] O. Bousquet and A. Elisseeff, Stability and generalization, The Journal of Machine Learning Research 2, 499 (2002).
- [59] H. Xu and S. Mannor, Robustness and generalization, Machine learning 86, 391 (2012).

- [60] P. L. Bartlett, D. J. Foster, and M. J. Telgarsky, Spectrally-normalized margin bounds for neural networks, Advances in neural information processing systems 30 (2017).
- [61] D. A. McAllester, Pac-bayesian model averaging, in Proceedings of the twelfth annual conference on Computational learning theory (1999) pp. 164–170.
- [62] S. Arora, R. Ge, B. Neyshabur, and Y. Zhang, Stronger generalization bounds for deep nets via a compression approach, in *International Conference on Machine Learning* (PMLR, 2018) pp. 254–263.
- [63] R. Giryes, A function space analysis of finite neural networks with insights from sampling theory, IEEE Transactions on Pattern Analysis and Machine Intelligence 45, 27 (2022).
- [64] J. Park and M. E. Newman, Statistical mechanics of networks, Physical Review E 70, 066117 (2004).

Supplemental Information: How accurate are neural approximations of complex network dynamics?

Vaiva Vasiliauskaite Computational Social Science, ETH Zürich, 8092 Zürich, Switzerland

Nino Antulov-Fantulin*

Computational Social Science, ETH Zürich & Aisot Technologies AG, Zürich, Switzerland (Dated: October 18, 2023)

I. NEURAL NETWORK MAPPINGS

Architecture of Differential Factorized Graph Neural Network We consider the following neural network model:

$$\dot{\mathbf{x}} = \boldsymbol{\psi}^{\ell}(\mathbf{x}) + \boldsymbol{\psi}^{\bigoplus} \left[\mathbf{A} \odot \left(\boldsymbol{\psi}^{q_1}(\mathbf{x})^{\top_1} \times_b \boldsymbol{\psi}^{q_2}(\mathbf{x})^{\top_2} \right) \right] (1)$$

where $\psi(\cdot)$ is a set of one or more hidden layers $\{\mathbf{h}^1, \mathbf{h}^2, ..., \mathbf{h}^N\}$ of the form:

$$\mathbf{h}^{i+1} = \sigma_i(\mathbf{h}^i \times_3 \mathbf{W}_i + \mathbf{b}_i),$$

$$\mathbf{h}^1 = \mathbf{x},$$

Where σ_i is an activation function.

Now we detail each function ψ and its effects on an input vector, layer by layer. We start with an input vector $\mathbf{x} \in \mathbb{R}^{n \times k}$. We add a dummy dimension $\mathbf{x} \in \mathbb{R}^{n \times k} \to \mathbf{x} \in \mathbb{R}^{n \times 1 \times k}$ to allow for tensor algebra. All dimensions are counted starting from 1.

- 1. $\boldsymbol{\psi}^{\ell}: \mathbb{R}^{n \times 1 \times k} \to \mathbb{R}^{n \times 1 \times k}$, consists of three layers. Layer 1: $\mathbf{W}_1 \in \mathbb{R}^{k \times h_1}$, $\mathbf{b}_1 \in \mathbb{R}^{1 \times h_1}$. \times_3 denotes 3-mode product of tensor with matrix i.e., $\mathbf{h}^1 \times_3 \mathbf{W}_1$ gives $\mathbb{R}^{n \times 1 \times k} \times_3 \mathbb{R}^{k \times h_1} \in \mathbb{R}^{n \times 1 \times h_1}$. Element-wise, $(\mathbf{h}^1 \times_3 \mathbf{W}_1)_{i,j,l} = \sum_m \mathbf{h}^1_{i,j,m} W_{m,l}$. The bias term $\mathbf{b}_1 \in \mathbb{R}^{1 \times h_1}$ is added via "broadcasted" operation, i.e. if our 3-mode product produced $\mathbf{a} \in \mathbb{R}^{n \times 1 \times h_1}$, then the total output is $\mathbf{c} = \mathbf{a} + \mathbf{b}_1$. Element-wise: $\mathbf{c}_{i,j,l} = \mathbf{a}_{i,j,l} + \mathbf{b}_{1,j,l}$. Lastly, σ_1 is a hyperbolic tangent function, also applied element-wise.
 - Layer 2: $\mathbf{W}_2 \in \mathbb{R}^{h_1 \times h_1}$, $\mathbf{b}_2 \in \mathbb{R}^{1 \times h_1}$, and σ_2 is hyperbolic tangent function, applied element-wise. After applying the 2^{nd} layer, we have a vector in $\mathbb{R}^{n \times 1 \times h_1}$.
 - Layer 3: $\mathbf{W}_3 \in \mathbb{R}^{h_1 \times k}$, $\mathbf{b}_3 \in \mathbb{R}^{1 \times k}$. and σ_3 is identity function. After applying the 3^{rd} layer, we have a vector in $\mathbb{R}^{n \times 1 \times k}$.
- 2. $\boldsymbol{\psi}^{q_1}, \boldsymbol{\psi}^{q_2}: \mathbb{R}^{n \times 1 \times k} \to \mathbb{R}^{n \times 1 \times h_2}$ consist of two layers. Layer 1: $\mathbf{W}_1 \in \mathbb{R}^{k \times h}$, $\mathbf{b}_1 \in \mathbb{R}^{1 \times h}$ and σ_1 is a hyperbolic tangent function. Layer 2: $\mathbf{W}_2 \in \mathbb{R}^{h \times h_2}$, $\mathbf{b}_2 \in \mathbb{R}^{1 \times h_2}$ and σ_2 is an identity function.

- 3. \mathbf{x}^{\top_1} denotes a transpose operations: $\mathbb{R}^{n \times 1 \times h_2} \to_{1,3} \mathbb{R}^{h_2 \times 1 \times n} \to_{2,3} \mathbb{R}^{h_2 \times n \times 1}$.
- 4. \mathbf{x}^{\top_2} denotes a transpose operation: $\mathbb{R}^{n \times 1 \times h_2} \to_{1,3} \mathbb{R}^{h_2 \times 1 \times n}$.
- 5. $(\boldsymbol{\psi}^{q_1}(\mathbf{x})^{\top_1} \times_b \boldsymbol{\psi}^{q_2}(\mathbf{x})^{\top_2})$: is a "batched" matrixmatrix product i.e. $\mathbb{R}^{h_2 \times n \times 1} \times_b \mathbb{R}^{h_2 \times 1 \times n} \in \mathbb{R}^{h_2 \times n \times n}$. If we have $A = B \times_b C$, where $B \in \mathbb{R}^{h_2 \times n \times 1}$ and $C \in \mathbb{R}^{h_2 \times 1 \times n}$, then element-wise we get $A_{i,j,l} = \sum_m B_{i,j,m} C_{i,m,l}$.
- 6. $\Phi \odot (\psi^{q_1}(\mathbf{x})^{\top_1} \times_k \psi^{q_2}(\mathbf{x})^{\top_2})$: $\mathbb{R}^{n \times n} \odot \mathbb{R}^{h_2 \times n \times n} \in \mathbb{R}^{h_2 \times n \times n}$. Here an operator \odot denotes a standard "broadcasted" element-wise multiplication. If we have $A = B \odot C$, $B \in \mathbb{R}^{n \times n}$, $C \in \mathbb{R}^{h_2 \times n \times n}$, we get $A_{i,j,l} = B_{j,l}C_{i,j,l}$.
- 7. $\psi^{\bigoplus}(\cdot)$, is composed of the following operations: invariant pooling and linear decoding.

 The invariant pooling layer is defined as a sum along the dimension 2: $\mathbb{R}^{h_2 \times n \times n} \to \mathbb{R}^{h_2 \times 1 \times n}$.

 After a transpose operation: $\mathbb{R}^{h_2 \times 1 \times n} \to_{1,3}$ $\mathbb{R}^{n \times 1 \times h_2}$, we apply a mapping from $\mathbb{R}^{n \times 1 \times h_2} \to \mathbb{R}^{n \times 1 \times k}$ via a single layer feedforward neural network with no activation functions.

We assumed that the function Q can be approximated by a product of two neural network functions. It is a reasonable assumption for factorizable Q, i.e. $Q(x_1,x_2)=q(x_1)q(x_2)$ (assuming k=1). Most of the dynamics we study in the paper are indeed factorizable, namely SIS, PD, MM, and MAK. One exception is Heat dynamics, which is factorizable only for homogeneous degree distributions. Nevertheless, our simulations show the described neural network model can also approximate Heat dynamics. More generally, one may consider a neural network of the following form

$$\dot{\mathbf{x}}_i = \boldsymbol{\psi}^{\ell}(\mathbf{x}_i) + \boldsymbol{\psi}^{\bigoplus} \left(\sum_{j: A_{ij} \neq 0} \boldsymbol{\psi}^{Q}(\mathbf{x}_i, \mathbf{x}_j) \right), \quad (2)$$

where ψ^Q acts on edges, and the 2nd term overall is a universal approximation of functions on edge sets [1, 2], while the 1st term is as before.

^{*} anino@ethz.ch

II. INDUCTIVE BIASES

Here we describe, in more detail, important inductive biases for using neural networks to learn dynamics in complex systems.

- 1. Size invariance: In Eq. 1 of the main text the functional forms of L, Q and \bigoplus are independent of the graph topology and the system size. Therefore, an appropriate neural network model would also be independent of the system size. Our proposed architecture adheres to this condition, as each function ψ is applied element-wise to each element of \mathbf{x} , namely $\mathbf{x}_i \in \mathbb{R}^k$.
- 2. Interactions: Any model defined as Eq. 1 of the main text consists of a sum of a self-interaction part that approximates $L(\cdot)$, and a neighbor interaction part that approximates $Q(\cdot, \cdot)$. Note that a single-layer GNN, such as a convolutional graph neural network, has no mixed quadratic terms $x_i x_j$ (a likely functional form of Q assuming k=1) and therefore does not simply satisfy such a condition. One could alternatively approximate these mixture terms with a wide single layer neural network, but this solution would disobey the requirement of size-invariance.
- 3. Network structure: We assume a known static network structure, upon which the dynamics unfold. The graph is represented as an adjacency matrix A. Incorporating graph structure into a model allows to efficiently evaluate each node's neighbourhood. We note that in the current work we assume a connected and undirected graph. We further assume that the graph structure is fully known. Future extensions of our work may explore the effects of incomplete knowledge of a graph structure, directionality and impact of the presence of multiple connected components. Lastly, one may consider, in the place of **A**, a single-layer graph convolution [3]. We do not consider such a neural architecture here: in our model, the graph acts as a scaffold. The simplest encoding of connectivity — the adjacency — is sufficient for our purposes.
- 4. Spatiotemporal locality: The dynamical process that follows Eq. 1 of the main text must be local, that is, the function $Q(\cdot,\cdot)$ encodes interactions between neighbours. However, including terms \mathbf{A}^{κ} in a multilayer graph neural network (as would be the case if we had multiple graph convolutional layers [2]) allows for κ -hop interactions via length κ walks in a network at a timescale smaller than the infinitesimal dt thereby subdividing dt to κ intervals and breaking an assumption of temporal locality.

Other constraints: Other constraints may be incorporated to achieve physical realism of a model. For example, if the system is closed, it does not exchange energy or mass with the environment, therefore $\sum_i \dot{x}_i(t) = C \quad \forall t$ (assuming k=1). A neural network can be weakly or strongly constrained to adhere to such conservation of a derivative. Furthermore, if Lipschitz continuity of \mathcal{F} is known, it can be used to regularize and potentially improve the neural approximation Ψ [4]. Note, that

Lipschitz continuity of the vector field \mathcal{F} is needed for the existence and uniqueness of ODE solution (see Picard–Lindelöf theorem [5]).

III. SIMULATION DETAILS

Dynamics The following parameters were used to simulate the dynamics.

- 1. **Heat**: B = 0.5.
- 2. **MAK**: B = 0.1, R = 1, F = 0.5.
- 3. **PD**: B = 2, R = 0.3, a = 1.5, b = 3.
- 4. **MM**: B = 4, R = 0.5, h = 3.
- 5. **SIS**: B = 4, R = 0.5.

Loss In all cases, during training we optimize an ℓ_1 loss function, summed over a set of inputs. To ensure equivalence across system and sample sizes, we report the node and sample average of this loss.

Training We used Adam optimizer with a learning rate 0.005 and weight decay 0.001. The training was done using batches of 50 samples unless otherwise stated. Graphs were sampled from an Erdös-Rényi ensemble with n=100 and edge probability p=0.1. For results presented in Sec. 4 of the main text, after 1000 epochs, we also used ReduceOnPlateau scheduler with the patience parameter set to 50 and the cooldown parameter set to 10.

Integration For numerical integration we used an explicit Runge-Kutta 5(4) method [6]. Implemented in TORCHDIFFEQ python package [7].

Figure 1 Main text: 10 overparameterized feedforward neural networks were trained with 251 parameters (h=10) each with 4 fully connected layers and Tanh activations. Each network was trained in 3000 epochs, using 40 bootstrapped samples from 50 total number of samples, using the learning rate of 0.003 and no weight decay. Samples were taken from a uniform distribution $\mathcal{U}[-2,2]$. The target function is $\mathcal{F}(x) = \cos(2x) + \mathcal{N}(0, \sigma = 0.01)$.

Table 2 main text, Fig. 3, Fig. 4: Neural networks were trained using 5000 samples from $\mathcal{U}(0,1)$ as inputs \mathbf{x} . The training was done in 2000 epochs, using the learning rate of 0.005, the weight decay of 0.001, using batch size of 50 out of the total number of 1000 training samples. The hidden layers have dimensions $h_1 = h = h_2 = 30$.

In the first three result columns from the left, the reported values are an average and a standard deviation across 10^3 samples. For the two right-most columns, the reported values are the mean and standard deviation over 100 random graphs, where for each graph, we compute the mean loss over 10^3 samples. In Fig. 3, the results for each parameter value of the beta distribution (a and b) are also averaged over 10^3 independent samples. In Fig. 4a) and c), the reported results are an average and

standard deviation across 10 graphs at each p (in a)) or n (in c)), where for each graph we computed the mean loss over 100 input samples from $\mathcal{U}(0,1)$. In Fig. 4b), the results are an average and standard deviation across 1000 samples from $\mathcal{U}(0,1) + \Delta$.

Neural networks studied Fig 2 main text: A total of 50 neural networks were trained, each with 90% of data and $h_1 = h = h_2 = 30$. For each dynamics, the full set of training data was obtained from 5 time series trajectories, $t \in [0,2]$, dt = 0.0101, amounting to a total number of 995 samples in the training dataset. The rest of the settings are as in the previous experiment.

Fig. 2a) The test graph is equivalent to the training graph. For a given Δ value, 10 independent time series trajectories were computed, starting from an initial value sampled from a shifted uniform distribution $\mathcal{U}(0,1) + \Delta$. For each initial value, a neural network prediction was computed by taking a random neural network from an ensemble and using it for integration. 100 samples $\mathbf{x}(t)$ from the predicted trajectory were then used to compute the distribution of the d-statistic. The d-statistic for the full sample (the null distribution) was evaluated by taking 100 samples from the training data. We used a statistical significance level of $\alpha = 0.05$ to compute the number of accepted datapoints by comparing the null distribution to the test distribution following Eq. 4 of the main text. The orange circles show the average and the standard deviation for accepted datapoints across the samples. The purple circles report the loss, Eq. 3, computed for each trajectory, averaged over trajectories.

Fig. 2b) We computed the d-statistic of the full sample and of the test sample in the same way, however now using 1000 draws for estimating the statistics. The figures show predicted trajectories computed using a random neural network from the ensemble. The title reports the fraction of datapoints that passed the significance test. Here the test graph is not equivalent to the training graph, but is sampled from and Erdös-Rényi ensemble with n=15, p=0.3.

Neural network from Fig 3 main text: In Fig. b) a neural network with $h_1 = h = h_2 = 20$ dimensions in their hidden layers, trained in 3000 epochs at a learning rate of 0.0001 with the weight decay of 0.001 and a batch size of 20. The training data were obtained from one time series trajectory \mathbf{x}_t . The initial value was sampled from a uniform distribution, and the solution was computed for an interval $t \in [0,1]$ using numerical integration with a timestep of 10^{-4} . We then sampled R = 100 timesteps from t, which represent timesteps t_r at which the signal was "measured". Lastly, we added normally distributed noise with $\sigma = 0.01$ to each training sample to obtain $\mathbf{z}(t_r)$. The setup was used to learn Heat dynamics with B = 1.5 on an ER graph with n = 10 nodes and 17 edges (p = 0.3). To test the effect of noise, we trained another neural network using the same data without observational noise. We then considered a test loss discussed in the main text, which we evaluated by drawing 1000 samples x from a uniform distribution. Lastly, we also

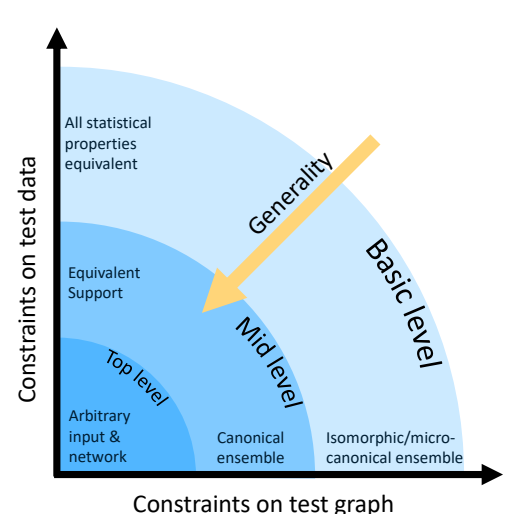


FIG. 1. 2D hierarchy of model generalization is defined by constraints imposed on the test data and the test graph as contrasted to the data and the graph used during training.

compared the observed losses for these two cases to the loss, observed in one untrained neural network.

IV. GENERALIZATION HIERARCHY

A trained model can be evaluated at several distinct levels of generality in two different directions: in terms of statistical properties of either the dataset \mathcal{D} , or the graph, mathematically represented as an adjacency matrix \mathbf{A} . In the main text, we proposed three tiers of generality in both directions. Fig. 1 illustrates the 2D hierarchy of model generalization.

V. SMALL EXAMPLE

To test our intuition about the neural network model, we first considered arguably the simplest graph dynamics in the simplest possible network: heat diffusion on a connected network of n=2 nodes. Both the train and test sets include 100 samples: $\psi_X \sim \mathcal{B}(5,2)$, whereas the test set is composed of a uniformly spaced set of points of a 2-dimensional lattice in the region [0,2]. As Fig. 2 shows, after 500 training epochs, the neural network approximates the state space well within the region of support of the beta distribution ([0,1]) even when $\psi_X \not\equiv \omega_X$, however does not generalize to regions of state space that are beyond the support of beta distribution. However, we observe a monotonic increase in loss as a function of distance from the training support.

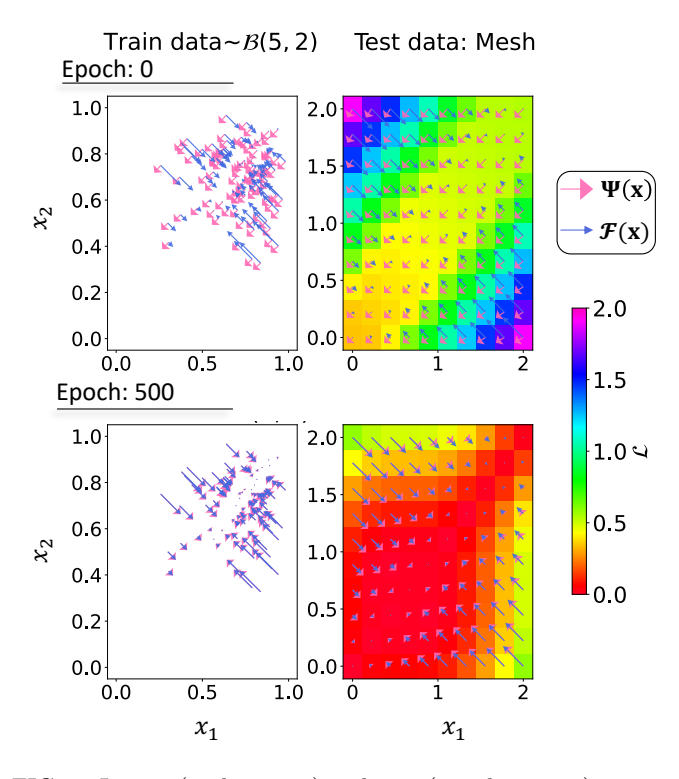


FIG. 2. Learnt (pink arrows) and true (purple arrows) vector field of diffusion dynamics on a connected n=2 node graph. The training sample are taken from a beta distribution $\mathcal{B}(5,2)$ and tested on a uniform lattice defined within range [0,2]. Color shows normalized ℓ^1 loss at a given square, calculated for a arrow that originates within this square.

VI. GENERALIZATION TO UNSEEN GRAPH ENSEMBLES AND INPUTS

Here we present more detailed results of generalization abilities of neural networks discussed in the main text. In all cases, the considered loss is

$$\mathcal{L} = \frac{1}{Z} \left[\mathbf{E}_{(\mathbf{x}, \mathbf{y}) \in \mathcal{D}} \| \mathcal{F}(x) - \mathbf{\Psi}(x) \|_{1} \right]$$
(3)

Generalization to unseen inputs within the training support First, we review the mid-level generalization in terms of statistical properties of input data. Since the neural networks were trained using samples from a uniform distribution $\mathcal{U}(0,1)$ with a support [0,1], then it is appropriate to study the mid-level generalization using distributions that have equivalent support. One such distribution is a beta distribution, parameterized by two real, positive numbers a and b, yielding samples within the same range of values, but a different density. In Fig. 3 we show the test loss $\mathcal{L}_{(a,b)}$ when inputs are sampled from a beta distribution with parameters a, b, as a fraction of training loss $(\mathcal{L}_{(1,1)})$. The figure shows that the neural approximation accuracy is within one order of magnitude from the loss achieved in train data, and sometimes, the test loss is even smaller than train loss. One exception is MAK dynamics, where we observe larger loss at lower

Dynamics	Graph	$\mathcal{L}_{ ext{self}}$	$\mathcal{L}_{ m nbr}$	
Heat	$\mathcal{G}\equiv\mathcal{H}$	3.46 ± 0.02	3.44 ± 0.13	
	$\mathcal{H} \sim \mathcal{P}(\mathfrak{G})$	3.46 ± 0.03	3.45 ± 0.15	
	$\mathcal{H} \sim \mathcal{P}(\mathfrak{H})$	3.46 ± 0.03	5.85 ± 0.72	
MAK	$\mathcal{G}\equiv\mathcal{H}$	5.99 ± 0.11	6.12 ± 0.44	
	$\mathcal{H} \sim \mathcal{P}(\mathfrak{G})$	5.98 ± 0.11	6.13 ± 0.48	
	$\mathcal{H} \sim \mathcal{P}(\mathfrak{H})$	5.98 ± 0.11	10.26 ± 2.07	
MM	$\mathcal{G}\equiv\mathcal{H}$	6.83 ± 0.08	6.9 ± 1.01	
	$\mathcal{H} \sim \mathcal{P}(\mathfrak{G})$	6.83 ± 0.08	6.91 ± 1.12	
	$\mathcal{H} \sim \mathcal{P}(\mathfrak{H})$	6.83 ± 0.08	8.88 ± 4.24	
PD	$\mathcal{G}\equiv\mathcal{H}$	10.33 ± 0.23	8.19 ± 0.83	
	$\mathcal{H} \sim \mathcal{P}(\mathfrak{G})$	10.32 ± 0.23	8.14 ± 0.89	
	$\mathcal{H} \sim \mathcal{P}(\mathfrak{H})$	10.33 ± 0.23	10.59 ± 1.75	
SIS	$\mathcal{G}\equiv\mathcal{H}$	7.84 ± 0.12	7.71 ± 0.14	
	$\mathcal{H} \sim \mathcal{P}(\mathfrak{G})$	7.85 ± 0.12	7.73 ± 0.15	
	$\mathcal{H} \sim \mathcal{P}(\mathfrak{H})$	7.84 ± 0.12	9.08 ± 0.86	

TABLE I. \mathcal{L}_{self} and \mathcal{L}_{nbr} for the two test graphs discussed in the Tab. 1 of the main text.

values of a. This result not only confirms that the generalization to a test data with different statistical properties is possible; it further indicates, intuitively, that the magnitude of loss is governed by the statistical properties of input data.

b. Generalization to unseen inputs outside the training support. In Fig. 4b), we study the top level generalization with respect to input range by drawing test samples from a uniform distribution and adding a constant Δ to each sample. Therefore at $\Delta \geq 1$ inputs are completely novel for our neural networks. The figure shows moderately small error when $\Delta < 1$, but the error increases drastically as inputs depart from a range observed during training. Furthermore, the quality of approximations is heterogeneous across different models of dynamics. In conclusion, how well a neural network model approximates beyond the training support depends on the dynamics.

c. Generalization to unseen graph densities In a similar way as for input data, we first consider mid-level generalization in terms of graph structure. Let us consider random Erdös-Rényi graphs $\mathcal H$ of various densities p but the same number of nodes as in the training network (n=100). The loss as a function of density is plotted in Fig. 4a). Again, there is a strong heterogeneity across dynamics, but generally we observe a correlation between density p and the loss.

As also mentioned in the main text, the dependence of loss on the density of a graph is likely a consequence of the accumulation of errors in the neighbor-interaction terms. Therefore, instead of looking at the discrepancy between \mathcal{F} and Ψ , we can also directly compare the loss observed in the approximation of the self-interaction term as well as in the neighbor-interaction term. In Tab. I, we consider these losses for the two test graphs discussed in the Tab. 1 of the main text. Specifically, let us define the

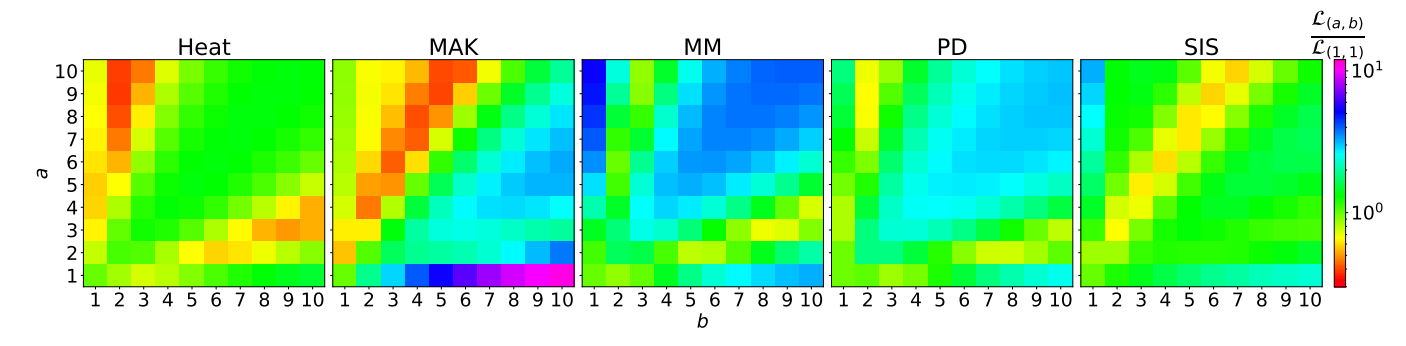


FIG. 3. Average sample and node loss $\mathcal{L}_{(a,b)}$ as a function of a, b that parameterize \mathcal{B} -distribution used to sample test datapoints \mathbf{x} . The values are divided by $\mathcal{L}_{(1,1)}$, i.e. the out-of-sample loss, evaluated on the samples taken from the same probability distribution function as that using which the neural network was trained.

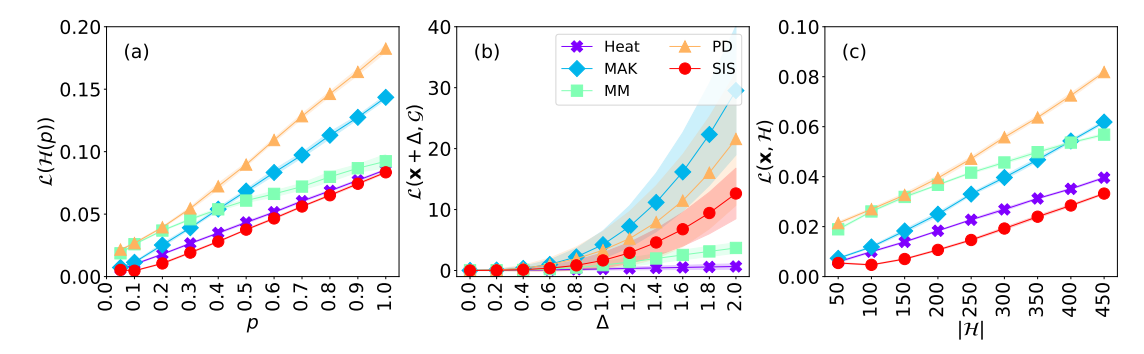


FIG. 4. Generalization is studied by analysing average sample and node loss $\langle \mathcal{L}(\mathcal{H}(p)) \rangle$ as a function of of **a**) p, the density of edges in the test network \mathcal{H} , **b**) Δ - a constant that shifts the neural network input by this amount outside the boundary of the seen distribution support from which **x** is sample and **c**) $|\mathcal{H}|$ the size of an input graph. The neural networks were trained using samples from uniform distribution and 10 different ER graphs \mathcal{G} , N = 10, $p \sim \mathcal{U}(0, 1)$.

loss in the self-interaction term as

$$\mathcal{L}_{\text{self}} = \frac{1}{Z} \left[\mathbf{E}_{(\mathbf{x}, \mathbf{y}) \in \mathcal{D}} \| L(\mathbf{x}) - \boldsymbol{\psi}^{\ell}(\mathbf{x}) \|_{1} \right], \tag{4}$$

and in the neighbor-interaction term as

$$\mathcal{L}_{nbr} = \frac{1}{Z} \left[\mathbf{E}_{(\mathbf{x}, \mathbf{y}) \in \mathcal{D}} \left\| \bigoplus_{j} A_{ij} Q(\mathbf{x}_{i}, \mathbf{x}_{j}) - \boldsymbol{\psi}^{\bigoplus} \left[\mathbf{A} \odot \left(\boldsymbol{\psi}^{q_{1}}(\mathbf{x})^{\top_{1}} \times_{b} \boldsymbol{\psi}^{q_{2}}(\mathbf{x})^{\top_{2}} \right) \right] \right\|_{1} \right].$$
 (5)

The Tab. I shows that the error in prediction of the self-interaction term is independent of the input graph. The loss in approximating the aggregate of neighbour interaction terms is statistically indistinguishable for a graph \mathcal{H} from the same canonical ensemble as the graph used in training ($\mathcal{H} \sim \mathcal{P}(\mathfrak{G})$), however, for a graph from a different ensemble, \mathcal{L}_{nbr} is larger than during training.

d. Generalization to unseen graph sizes Lastly, in Fig. 4c) we keep the original network density (p=0.1) but increase the network size. As before, we observe a monotonic increase in the loss with the network size. We theorize that these correlations between the graph density and the loss, as well as the graph size and the loss, are a consequence of accumulation of errors in the

approximation of neighbour interactions term. More specifically, since the self-interaction and the neighbour-interaction terms are used only in a superposed way, the self-interaction term may be used to correct some inaccuracies in the approximation of the neighbour-interaction term, and vice versa. In particular, separating the self-interaction and the neighbour-interaction terms from their superposition is an example of blind-source separation problem [8].

VII. USE OF REAL DATA – GRADIENT LEARNING DETAILS

In the example discussed in Sec. V of the main text, we use a forward computational graph with an automatic differentiation [9]. Here we derive the computational graph and its gradient computation.

For simplicity, let us assume a scalar variable, i.e. d=1 and that its ground truth trajectory is $\{x_r\}$, where index r denotes specific times $\{t_0, t_1, ..., t_R\}$ at some irregular time samplings. We also assume that observations are corrupted with additive noise: $z[x_r] = x_r + \epsilon_r$, where $\epsilon_r \sim \mathcal{N}(0,\sigma)$. A neural network represents a scalar function $\Psi: \mathbb{R}^1 \to \mathbb{R}^1$ and is parameterized with weights w. The goal of learning is finding parameters w that minimize

the following objective:

$$\bar{\mathcal{L}} = \sum_{r=0}^{R} \mathcal{L}(z[x_r], \hat{x}_r)$$

$$= \sum_{r=0}^{R} \mathcal{L}\left(x_r + \epsilon_r, x_{r-1} + \epsilon_{r-1} + \int_{t_{r-1}}^{t_r} \Psi(\hat{x}(\tau)) d\tau\right).$$
(6)

As in regular non-convex optimization, the weights are updated according to the following rule:

$$w_k^{l+1} = w_k^l - \eta \frac{\partial \bar{\mathcal{L}}(\hat{x}_r, z[x_r]; w)}{\partial w_k},$$

$$= w_k^l - \eta \sum_{r=0}^R \frac{\partial \mathcal{L}(\hat{x}_r, z[x_r]; w)}{\partial w_k},$$
(7)

where η is a learning rate and l is a training step. Let us first find an expression of the derivative for \mathcal{L} :

$$\frac{\partial \mathcal{L}(\hat{x}_r, z[x_r]; w)}{\partial w_k} = \frac{\partial \mathcal{L}(\hat{x}_r, z[x_r]; w)}{\partial x_r} \frac{\partial \hat{x}_r}{\partial w_k}.$$
 (8)

To compute Eq. 8, let us subdivide an interval $[t_{r-1}, t_r]$ into N intervals, each of granularity $\Delta t = (t_r - t_{r-1})/N$ as follows: $\{t_{r,j}\}_{j=0}^N$, where $t_{r,j} = t_{r-1} + j\Delta t$. The dynamics of \hat{x}_r is

$$\hat{x}_r = \hat{x}_{r,N} = \hat{x}_{r,N-1} + \Delta t \, \Psi_{r,N-1} \Psi_{r,N-1} = \Psi(\hat{x}_{r,N-1}),$$

which means that $\hat{x}_{r,N}$ is a function of two variables, $\hat{x}_{r,N} = f(\hat{x}_{r,N-1}, \Psi_{r,N-1})$. The derivative of \hat{x}_r therefore is

$$\frac{\partial \hat{x}_{r,N}}{\partial w_k} = \frac{\partial \hat{x}_{r,N}}{\partial \hat{x}_{r,n-1}} \frac{\partial \hat{x}_{r,N-1}}{\partial w_k} + \frac{\partial \hat{x}_{r,N}}{\partial \Psi_{r,N-1}} \frac{\partial \Psi_{r,N-1}}{\partial w_k}.$$

Since $\frac{\partial \hat{x}_{r,N}}{\partial \hat{x}_{r,N-1}} = 1$ and $\frac{\partial \hat{x}_{r,N}}{\partial \Psi_{r,N-1}} = \Delta t$, we get

$$\frac{\partial \hat{x}_{r,N}}{\partial w_k} = \frac{\partial \hat{x}_{r,N-1}}{\partial w_k} + \Delta t \frac{\partial \Psi_{r,N-1}}{\partial w_k},$$

which is a recurrence relation

$$\frac{\partial \hat{x}_{r,N}}{\partial w_k} = \sum_{i=0}^{N-1} \Delta t \frac{\partial \Psi_{r,j}}{\partial w_k}.$$
 (9)

Note that $\frac{\partial \hat{x}_{r,0}}{\partial w_k} = \frac{\partial \hat{x}_{r-1}}{\partial w_k} = 0$, since $\hat{x}_{r,0}$ is by definition "a temporary initial condition" for a segment $[t_{r-1}, t_r]$. By substituting Eq. 9 back to the Eq. 8, we get

$$\frac{\partial \mathcal{L}(\hat{x}_r, z[x_r]; w)}{\partial w_k} = \frac{\partial \mathcal{L}(\hat{x}_r, z[x_r]; w)}{\partial \hat{x}_r} \sum_{j=0}^{N-1} \Delta t \frac{\partial \Psi_{r,j}}{\partial w_k}, \quad (10)$$

where $\frac{\partial \Psi_{r,j}}{\partial w_k}$ is just the regular gradient of differentiable neural network $\Psi_{r,j} = \Psi(\hat{x}_{r,j}; w)$. Putting Eq. 10 back to the Eq. 7, we get that weights are updated as follows:

$$w_k^{l+1} = w_k^l - \eta \sum_{r=0}^R \frac{\partial \mathcal{L}(\hat{x}_r, z[x_r]; w)}{\partial \hat{x}_r} \sum_{j=0}^{N-1} \Delta t \frac{\partial \Psi_{r,j}}{\partial w_k}.$$
 (11)

From Eq. 11, one can see how observational noise affects the computation of the gradient: it affects only the derivative of the loss w.r.t. \hat{x}_r . E.g. in case \mathcal{L} is computed using ℓ^2 norm: $\mathcal{L}(\hat{x}_r, z[x_r]; w) = (\hat{x}_r - z[x_r])^2$, we get $\frac{\partial \mathcal{L}(\hat{x}_r, z[x_r]; w)}{\partial \hat{x}_r} = 2(\hat{x}_r - z[x_r])$. For ℓ^1 norm, $\mathcal{L}(\hat{x}_r, z[x_r]; w) = |\hat{x}_r - z[x_r]|$, we get $\frac{\partial \mathcal{L}(\hat{x}_r, z[x_r]; w)}{\partial \hat{x}_r} = \operatorname{sgn}[\hat{x}_r - z[x_r]]$ for $\hat{x}_r \neq z[x_r]$.

- E. Wagstaff, F. B. Fuchs, M. Engelcke, M. A. Osborne, and I. Posner, Universal approximation of functions on sets, The Journal of Machine Learning Research 23, 6762 (2022).
- [2] K. Xu, S. Jegelka, W. Hu, and J. Leskovec, How Powerful are Graph Neural Networks?, 7th International Conference on Learning Representations, ICLR 2019 10.48550/arxiv.1810.00826 (2018).
- [3] T. N. Kipf and M. Welling, Semi-supervised classification with graph convolutional networks, arXiv preprint arXiv:1609.02907 (2016).
- [4] H. Gouk, E. Frank, B. Pfahringer, and M. J. Cree, Regularisation of neural networks by enforcing Lipschitz continuity, Machine Learning 110, 393 (2021).

- [5] E. A. Coddington, N. Levinson, and T. Teichmann, Theory of ordinary differential equations (1956).
- [6] L. F. Shampine, Some practical runge-kutta formulas, Mathematics of Computation 46, 135 (1986).
- [7] R. T. Q. Chen, torchdiffeq (2018).
- [8] S. Choi, A. Cichocki, H.-M. Park, and S.-Y. Lee, Blind source separation and independent component analysis: A review, Neural Information Processing-Letters and Reviews 6, 1 (2005).
- [9] A. G. Baydin, B. A. Pearlmutter, A. A. Radul, and J. M. Siskind, Automatic differentiation in machine learning: a survey, Journal of Marchine Learning Research 18, 1 (2018).